RSC Applied Polymers

PAPER

View Article Online
View Journal | View Issue

Cite this: *RSC Appl. Polym.*, 2025, **3**, 1564

Design of a dual dynamic elastomeric vitrimer based on disulfide metathesis and transesterification reactions

Bhavya Parameswaran,[a] Tuhin Subhra Pal[a] and Nikhil K. Singha *[a,b]

Received 2nd May 2025,
Accepted 1st September 2025

DOI: 10.1039/d5lp00127g

rsc.li/rscapplpolym

Vitrimers represent a promising class of new-generation materials with covalent adaptive networks (CANs) based on an associative exchange mechanism. Herein, we utilised epoxy-functionalized elastomers, like poly(ethylene-*co*-vinyl acetate-*co*-glycidyl methacrylate) (EVA-GMA), for designing a dual dynamic network based on β-hydroxyl ester linkage as well as disulfide metathesis reactions, which were enabled by a new crosslinker, succinic anhydride-modified 4-aminophenyl disulfide (SA-APDS), which has a disulfide linkage in the backbone and a –COOH group at the *para* position. These dynamic linkages are capable of undergoing exchange reactions at elevated temperatures, thereby allowing the rearrangement of the network topology and exhibiting vitrimer-like behaviour. The resultant elastomeric vitrimer exhibits good mechanical performance, including a tensile strength of ~6.1 MPa and elongation at break up to 1300%, demonstrating super-elastomeric characteristics. Interestingly, the elastomeric vitrimer showed fluorescence behaviour due to the presence of a conjugated system in the new crosslinker. The ability of this material to maintain and reconfigure crosslink density through dual associative mechanisms showed that vitrimer-like materials have self-healing, recyclable, and reprocessable characteristics. Stress relaxation experiments confirmed the vitrimeric behaviour with an activation energy of 46.8 kJ mol^{-1} and a vitrification temperature of 83 °C. This new vitrimeric elastomer, with fluorescence characteristics, can have potential applications in areas where a unique combination of mechanical and optical properties is necessary.

Introduction

Elastomers are an important class of polymer materials that are indispensable in our daily lives due to their broad range of applications.[1–3] They are predominantly crosslinked with sulphur as invented by Charles Goodyear in 1834 or by using peroxides, metal oxides, resins, *etc*. The crosslinks formed by these conventional methods are irreversible, due to which it is difficult to recycle, reprocess, and reuse elastomers.[4] These issues pose a significant challenge to the environment when it comes to the matter of disposal and waste management. Hence, there is a crucial need for the development of more environmentally friendly materials with strong economic prospects of reusability.

Incorporating dynamic covalent networks is an interesting approach, as they can undergo reversible covalent bond formation and cleavage, enabling them to adapt their properties and respond to external stimuli. For elastomeric materials, this self-repairing process can take place through either an associative bond exchange or a dissociative bond exchange pathway. Associative exchangeable bonds belong to the class of self-healing elastomers, which can form associative crosslinks after a fracture or damage while maintaining constant crosslinking density throughout the healing process.[5] Some of the important examples of associative bond exchange reactions are transesterification,[6–8] disulfide metathesis,[9,10–12] olefin metathesis,[13] transamination,[14] *etc*. Dissociative exchangeable bonds represent a versatile class of dynamic material systems. One of the prominent examples of dissociative exchangeable bonds is the Diels–Alder chemistry.[15–17] Reversible networks based on supramolecular interactions rely on non-covalent bonds such as hydrogen bonding,[18,19] metal coordination,[20] π–π stacking[21] or host–guest interactions.[22] These dynamic interactions enable the material to respond to external stimuli, making the networks reversible, self-healing, and adaptable.

Vitrimers, as coined by Leibler *et al.*, are an attractive subset of dynamic covalent networks with associative exchangeable bonds and are expected to present a new paradigm for developing reusable elastomeric materials, as they can rearrange the network topology at higher temperatures

[a]*Rubber Technology Centre, Indian Institute of Technology Kharagpur, West Bengal 721302, India. E-mail: nks@rtc.iitkgp.ac.in, nks8888@yahoo.com*
[b]*School of Nano Science and Technology, Indian Institute of Technology Kharagpur, West Bengal 721302, India*

and maintain the same degree of crosslinking even in a recycled state.[23] These materials have an interesting property, that is, the crosslinked material can maintain its structural integrity even after it is reprocessed.[7,8,24,25] Leibler *et al.*[23] first demonstrated vitrimers by crosslinking diglycidyl ether of bisphenol A with glutaric anhydride and zinc acetylacetonate as the catalyst. There has been tremendous interest in this new class of materials since the last decade.[26,27]

Recent literature has extensively explored vitrimers derived from disulfide metathesis and transesterification for the crosslinking of epoxy resins, as well as other low molecular weight compounds containing epoxy groups. Zhang *et al.* demonstrated rapid stress relaxation in an epoxy resin based on bisphenol A crosslinked by β-hydroxy ester linkages and disulfide metathesis.[28] In this case, an aliphatic disulfide with a carboxylic acid at each end was utilised as the crosslinker, which endowed the crosslinked epoxy resin with rapid stress relaxation ranging from 1.5 s (200 °C) to 5500 s (60 °C). Vilanova-Pérez *et al.*[29] synthesised two UV-curable vitrimeric materials based on ethylene glycol phenyl ether methacrylate (EGPMA) and poly(ethylene glycol) methyl ether methacrylate (PEGMA) using an aliphatic compound containing disulfide as well as β-hydroxy ester linkages as the crosslinking agent. Both the materials exhibited near-ambient glass transition temperatures (T_g) and excellent vitrimeric behaviour, with rapid stress relaxation and low activation energies, and showed higher topology freezing temperatures (T_v) than T_g, suggesting potential for shape-memory applications. Wang *et al.*[30] synthesised an extended epoxy resin network based on bisphenol A by reacting it with suberic acid to incorporate the β-hydroxy ester linkages, and was then crosslinked with an aromatic disulfide. These materials showed excellent self-healing properties. Huang *et al.*[31] developed a vitrimer containing epoxy resin based on bisphenol A crosslinked with 2,2′-dithiobenzoic acid, where the dynamic crosslinker had an aromatic disulfide with a –COOH group at the *ortho* position. The material showed vitrimeric behaviour with potential application as a high-performance adhesive.

Chen *et al.*[32] utilized TEMPO-oxidised cellulose nanocrystals [TOCNS] as a covalent crosslinking agent and a reinforcement in epoxidised natural rubber (ENR). Lin *et al.*[33] developed a recyclable and self-healable ENR-based composite by incorporating a citric acid-modified bentonite composite. Lin *et al.* reported the vitrimer behaviour of the reactive blend of ENR/XNBR without the aid of any external crosslinker.[34] Zhang *et al.*[35] developed a malleable, strong and reversible ENR composite by blending it with carboxyl-functionalised carbon nanodots. Liu *et al.*[6] covalently crosslinked ENR with sebacic acid before grafting *N*-acetyl glycine to simultaneously produce hydroxy ester linkages and amide groups. Cao *et al.*[36] developed an ENR-based vitrimer-like elastomer with high self-healing efficiency. In that work, the hydroxyl groups on cellulose nanocrystals (CNCs) were converted into carboxyl groups by 2,2,6,6-tetramethylpiperidinyl-1-oxyl radical (TEMPO)-mediated oxidation and incorporated into ENR rubber. Thus, in most of the literature reports, mostly ENR-based vitrimer-like materials have been prepared using a single system of transesterification of β-hydroxy ester linkages.

Ethylene-vinyl acetate (EVA) copolymers are an important class of polymers, which can be thermoplastic or elastomeric depending on the content of vinyl acetate (VA).[1] Because of its unique properties, like resistance to UV radiation, oil, heat ageing and excellent flexibility, EVA is widely used in automotive parts, shoes, adhesives, coatings, *etc*. Recently, in EVA elastomers, a few percent of a third monomer, glycidyl methacrylate (GMA), has been introduced to incorporate the epoxy functionality as a pendant group.[1]

In this study, we have developed a new elastomeric vitrimer using the epoxy functionality in EVA-GMA based on a dual dynamic network using metathesis reactions of disulfides as well as transesterification of β-hydroxy ester linkages. In this case, we have synthesised a new dual dynamic crosslinker with a disulfide linkage in the middle and dicarboxylic acid as the end group, capable of targeting the epoxy groups in EVA-GMA. The choice of synthesising an aromatic disulfide containing crosslinker with the carboxyl groups at the *para* position was made due to the more favourable geometry and reduced steric hindrance, as the *para* configuration allows stable and more commending exchange reactions between the disulfide groups.[37] Also, the aromatic disulfides benefit from electron delocalization due to the conjugation between the sulfur atoms and the aromatic ring. The resonance effect in aromatic systems can help stabilise the disulfide bond, making it more thermodynamically favourable for breaking and reformation during exchange reactions.[38] Herein, we explored a rather inexpensive route to synthesise the aromatic disulfide containing *para*-carboxylic acid. To the best of our knowledge, there is no report on the development of a vitrimer-like elastomer based on EVA-GMA, utilising a dual dynamic metathesis mechanism based on disulfide metathesis as well as β-hydroxy ester exchange reactions. The reaction between the epoxy groups and the carboxylic acid moieties results in the formation of β-hydroxy ester linkages, which are known to promote transesterification reactions at elevated temperatures, thereby enabling network topology rearrangement and conferring vitrimer-like properties.

The reversible nature of disulfide bond exchange is well established, enabling the creation of dynamic, responsive materials capable of undergoing structural rearrangements in response to external stimuli. The synergistic effect of the β-hydroxy ester and disulfide linkages endows the crosslinked elastomer with improved mechanical as well as vitrimer-like properties. Additionally, the material exhibited fluorescence behaviour, along with excellent vitrimeric characteristics of self-healing and recyclability.

Experimental

Materials

The EVA-GMA terpolymer under the trade name of Levapren® NPG VP was supplied by Arlanxeo, Germany. This elastomer is a random terpolymer of ethylene, vinyl acetate (VA) and glyci-

dyl methacrylate (GMA) monomer units with a VA content of 60 wt%, ethylene content of 37 wt% and GMA content of 3 wt%. 4-Aminophenyl disulfide (APDS), succinic anhydride (SA) and 1,4-phenylenediamine (AP) were purchased from TCI Chemicals. The catalyst 1,5,7-triazabicyclo [4.4.0] dec-5-ene (TBD) was purchased from Sigma Aldrich, USA. Solvents like diethyl ether and dimethylformamide (DMF) were purchased from Merck.

Characterisation and analyses

Nuclear magnetic resonance (NMR) analysis. NMR analysis was carried out using a Bruker 600 MHz instrument. The solvent used was DMSO-d_6, and the analysis was carried out at room temperature.

Matrix-assisted laser desorption ionization time-of-flight mass spectrometry (MALDI-TOF-MS). MALDI-TOF-MS analysis was carried out with an UltrafleXtreme mass spectrometer (Bruker), employing 2,5-dihydroxybenzoic acid (DHB) as the matrix and sodium trifluoroacetate as the cationizing agent.

Fourier transform infrared spectroscopy (FTIR). The modification of various functional groups of the elastomer was determined using FTIR spectroscopy (PerkinElmer, model spectrum-2, Singapore) in the scanning range from 400 to 4000 cm^{-1} in attenuated total reflectance (ATR) mode. The number of scans was set to 16 for each sample.

Differential scanning calorimetry (DSC). DSC analysis was carried out on a TA DSC (Discovery 25) instrument at a heating rate of 10 °C min^{-1} and a temperature range from −80 to 200 °C under a nitrogen atmosphere.

Thermogravimetric analysis (TGA). The thermal degradation profile of various samples was analysed using a TGA-50 series (Shimadzu) instrument. The experiment was carried out by gradually heating approximately 10 mg of sample from ambient temperature to 800 °C at 20 °C min^{-1} under a N_2 atmosphere.

Nanoindentation experiments

The hardness of crosslinked samples with different dynamic and non-dynamic crosslinkers was determined using a TI 950 TriboIndenter (Hysitron Inc., USA) with a constant load of 50 μN under ambient conditions. The samples were mounted on glass slides and were attached using tape on the edges. An average of ten measurements were recorded for each sample.

Optical microscopy

The self-healing behaviour of the crosslinked samples was determined using a scratch and heal test. A sharp cut was made on the crosslinked sample using a scalpel, and it was placed at 120 °C for 120 min. A Cilika benchtop optical microscope (OM) was used to investigate the "scratch and heal test" of the cut and healed samples.

UV-Vis spectroscopy

A UV–Vis absorption spectrometer (PerkinElmer (Lambda 35)) was used to study the absorption spectra of the prepared samples in both solid and liquid forms in the wavelength range from 200 cm^{-1} to 700 cm^{-1} at ambient temperature. The sample thickness was maintained at ~0.1 mm for solid-state absorption.

Fluorescence spectroscopy

The fluorescence behaviour of the crosslinked samples was characterised using a Shimadzu RF-6000 spectrofluorophotometer.

Time-resolved photoluminescence spectroscopy (TRPL)

The decay profile was obtained using a PicoQuant PL spectrophotometer with a 405 nm diode laser as the source of excitation.

Dynamic bond recovery test

The phenomenal stress relaxation experiments were carried out to estimate the rate of dynamic bond recovery using an Anton Paar MCR 102. Rectangular specimens with a length of 40 mm, width of 10 mm and thickness of 1 mm were used.

Mechanical properties

The tensile properties of the samples were obtained using a Hounsfield Universal Testing Machine (UTM) following the ASTM D412 standard. The analysis was carried out using a 10 kN load at a rate of 50 mm min^{-1} until the specimen failed.

Crosslinking density

The crosslinking density of the crosslinked samples using different crosslinkers was determined using the Flory–Rehner equation.[39] The disc-shaped samples were immersed in 3 mL of toluene for 72 h at room temperature to attain equilibrium swelling. The weight of the swollen sample was noted and denoted as W_1. Furthermore, the swollen sample was placed in a vacuum oven at 50 °C overnight for drying, and the dried weight is denoted as W_2. The following equation was used to calculate the crosslinking density (eqn (1)).

$$\mathrm{CLD} = -\frac{1}{V_s}\left[\frac{\ln(1-V_R)+V_R+\chi V_R}{{V_R}^{1/3}}\right] \quad (1)$$

wherein V_R can be calculated using eqn (2)

$$V_R = \frac{W_3}{W_3 + (W_2 - W_3)\rho/\rho_s} \quad (2)$$

wherein, CLD is the crosslinking density in mol cm^{-3}, V_R is the volume fraction of the crosslinked elastomer in the swollen state, V_s is the molar volume of toluene, 105.9 mL mol^{-1} at r.t., ρ is the density of the crosslinked elastomer, and ρ_s is the density of toluene (0.87 g mL^{-1}). χ = 0.033 is the interaction parameter between EVA-GMA elastomer and toluene, and it was calculated from the Flory–Huggins interaction parameter relation (eqn (3)).

$$\chi = 0.487 + 0.228V_R. \quad (3)$$

Sol–gel analysis

The extent of crosslinking in the elastomer networks was assessed *via* sol–gel analysis. Approximately, 100 mg of the

crosslinked sample was weighed (W_0) and immersed in 30 mL of DMF at room temperature for 48 h. The solvent was refreshed every 12 h to ensure extraction of soluble components. After extraction, the samples were filtered and dried under vacuum at 60 °C to a constant weight (W_f). The gel fraction (%) was calculated using eqn (4).[40]

$$\text{Gel fraction } (\%) = W_f/W_0 \times 100. \quad (4)$$

Synthesis of the dual dynamic crosslinker, [4,4′-((disulfanediylbis(4,1-phenylene))bis(azanediyl))bis(4-oxobutanoic acid)] or succinic anhydride-modified 4-aminophenyl disulfide (SA-APDS)

In a typical synthetic procedure, 1 g (4.025 mmol) of 4-aminophenyl disulfide (APDS) was dissolved in dimethylformamide (DMF) at room temperature (RT). Following the dissolution, 0.80 g (8.05 mmol) of succinic anhydride (SA) was added to the reaction mixture, which was then stirred for 16 h at RT (as illustrated in Scheme S1). Upon completion of the reaction, the resultant solution was precipitated by adding diethyl ether, and the precipitate was collected through filtration. The white solid obtained was subsequently dried in an air oven at 60 °C for 24 h to ensure complete removal of any residual solvents.

^{1}H NMR in DMSO-d_6: δ (ppm) = 12.15 (–COOH–), 10.12 (–CONH–), 7.69 and 7.49 (phenyl protons), 2.56 and 2.55 (methyl protons) (Fig. S1). The molecular mass obtained from MALDI-TOF mass spectrometry is 448.6 g mol^{-1}, as correlated with the isotopic distribution calculation[41] (Fig. S2). FTIR (cm^{-1}) (Fig. S3): 1580 (NH bending of the amide group), 1715 (C=O stretching of the carboxyl group) and 3400 (OH stretching). Thermogravimetric analysis (TGA) and differential thermogravimetry (DTG) plots of the synthesized dual dynamic crosslinker revealed a distinct two-step degradation profile of –COOH and S–S groups at 230–330 °C and C–C linkages at 460 °C, as illustrated in Fig. S4.

Modification of EVA-GMA with the dual-dynamic crosslinker

In a dry 50 mL round-bottom flask, approximately 5 g of EVA-GMA (containing 1.02 mmol of reactive GMA units) was dissolved in dimethylformamide (DMF) at room temperature. An equimolar amount of the dual dynamic crosslinker and the epoxy content in the EVA-GMA elastomer, along with 0.02 g (0.2 mol) of 1,5,7-triazabicyclo [4.4.0] dec-5-ene (TBD), a transesterification catalyst, were separately dissolved in 2 mL of DMF. This solution was then added dropwise to the elastomer under a nitrogen atmosphere at room temperature. The resulting mixture was subjected to continuous stirring on a magnetic stirrer at 110 °C for 24 h. Following the reaction, the dark-brown polymer solution obtained was cast on a Teflon Petri dish and subsequently placed in an air oven at 50 °C for 3 days to form a dried film. This sample was designated as E_1 for subsequent analyses. Similarly, EVA-GMA was modified with APDS and AP, and the samples were designated as E_2 and E_3, respectively.

A model reaction between EVA-GMA and 2-furoic acid

To confirm the occurrence of the epoxy acid reaction and to rule out the possibility of excess vinyl acetate groups in the EVA-GMA rubber reacting with the acid groups of the crosslinker, a model study was carried out. In this case, 0.5 g of the EVA-GMA elastomer containing 1.02 mmol of reactive GMA units was dissolved in 5 mL of DMF in a two-neck round-bottom flask. Furthermore, an equimolar amount of 2-furoic acid (11 mg, 0.098 mmol) along with the TBD catalyst was dissolved in DMF and added to the rubber solution under a nitrogen atmosphere. The resultant mixture was subjected to continuous stirring on a magnetic stirrer at 110 °C for 36 h and was further dried in an air oven at 50 °C for 2 days.

Results and discussion

In this case, the EVA-GMA elastomer was first modified using succinic anhydride-modified 4-aminophenyl disulfide (SA-APDS), as shown in Scheme 1. This SA-APDS was synthesized by reacting APDS with succinic anhydride, as shown in Scheme S1.

SA-APDS acted as a dual dynamic crosslinker through its disulfide linkages, leading to a disulfide metathesis reaction, and through its COOH groups, leading to the β-hydroxy ester metathesis reaction with epoxy groups in EVA-GMA. In general, the epoxy groups are highly reactive due to their strained three-membered oxirane ring structure, which makes them more susceptible to nucleophiles like carboxylic acids. To confirm the occurrence of the epoxy acid reaction and to rule out the plausible transesterification reaction between the –COOH groups in the crosslinker and excess vinyl acetate groups in the EVA-GMA rubber, a model study was carried out by reacting the pristine elastomer with 2-furoic acid

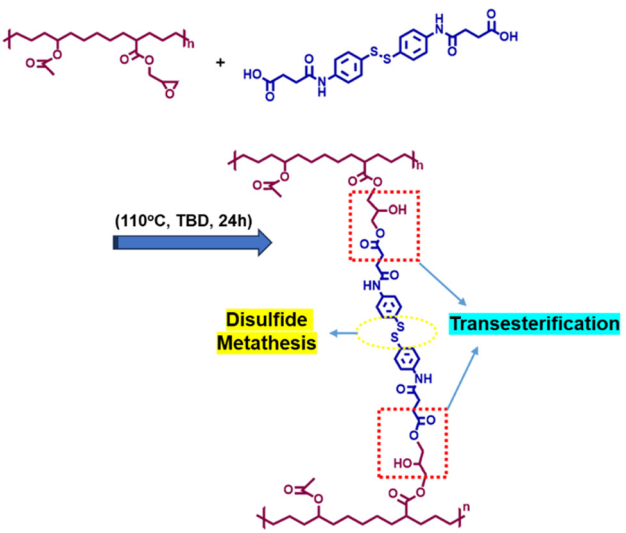

Scheme 1 Schematic representation of crosslinking in EVA-GMA with the dual dynamic crosslinker.

(Scheme S2). In this case, we used furoic acid as the model acid for this control study because its aromatic protons will be observed distinctly in the aromatic region for an efficient quantification study.

The opening of epoxy pendants of the EVA-GMA elastomer with 2-furoic acid catalysed by TBD, forming β-hydroxy esters, was confirmed by NMR analysis (Fig. S4). The GMA content (with epoxy pendant groups) in the EVA-GMA elastomer was found to be 2.9 wt%, displaying distinct resonances at δ (ppm) = 2.65 (H^1), 2.85 (H^1), and 3.21 (H^2), which correspond to the protons of the epoxy group in the pristine elastomer (Fig. S4a). Fig. S4b presents the ^{1}H NMR spectrum of EVA-GMA grafted with 2-furoic acid. After modification with 2-furoic acid, the signals corresponding to oxirane (CH_2) protons at δ (ppm) 2.65, δ (ppm) 2.85 and δ (ppm) 3.21 completely disappeared. This indicates complete modification of the pendant oxirane protons through grafting with the acid group. The appearance of an OH proton at δ (ppm) = 3.64(H^{14}) in the modified elastomer confirms the formation of hydroxyl groups due to the epoxy-acid reaction, which forms β-hydroxy esters. The methyl protons at δ (ppm) 2.07 (H^6) and δ (ppm) 4.95 (H^7) corresponding to the vinyl acetate groups remained intact or there is no change in their peak intensity, which confirms the non-participation of vinyl acetate groups in the transesterification reaction.

To evaluate the impact of the dual dynamic crosslinker on EVA-GMA rubber, two control samples were prepared under identical reaction conditions (Scheme 2).

The first control, E_2, involved crosslinking EVA-GMA with an equimolar amount of APDS in relation to the GMA content, resulting in a dynamically crosslinked elastomer characterized by reversible disulfide linkages. For the second control, E_3, AP was used for crosslinking EVA-GMA under the same conditions, thereby creating an epoxy–amine crosslinking system devoid of reversible linkages.

The correlation between the crosslinking of the pristine elastomer and the incorporation of the dual dynamic crosslinker was thoroughly investigated using FTIR spectroscopy (Fig. 1). Notably, the attenuation of the characteristic epoxy stretching vibrations at 830 and 851 cm^{-1} in sample E_1, compared to the unmodified EVA-GMA elastomer, provides definitive evidence of epoxy ring opening and the subsequent formation of β-hydroxy ester linkages. The observed increase in absorption intensity at 1730 cm^{-1} is indicative of the formation of β-unsaturated ester functionalities. The C–N stretching vibration, attributed to the crosslinker, is detected at 1498 cm^{-1}.[42] Additionally, the N–H bending vibration, corresponding to the formation of amide linkages present in the dual dynamic crosslinker which was formed during the condensation reaction of APDS and SA, is observed at 1530 cm^{-1} in sample E_1, further supporting the successful incorporation of the dual dynamic crosslinker.

Fig. 2 shows the comparative FTIR spectra for samples E_1, E_2, and E_3, which reveal a broad absorption band at 3300–3500 cm^{-1} in all three samples, which corresponds to the presence of hydroxyl groups formed during the epoxy ring opening by the carboxyl group in E_1 as well as due to N–H stretching. This spectral feature confirms the occurrence of transesterification reactions, as evidenced by the epoxy ring opening and the subsequent formation of β-hydroxy ester linkages. Furthermore, the spectra of samples E_1, E_2, and E_3 exhibit N–H stretching vibrations at 3460 cm^{-1}, associated with the presence of amine groups.

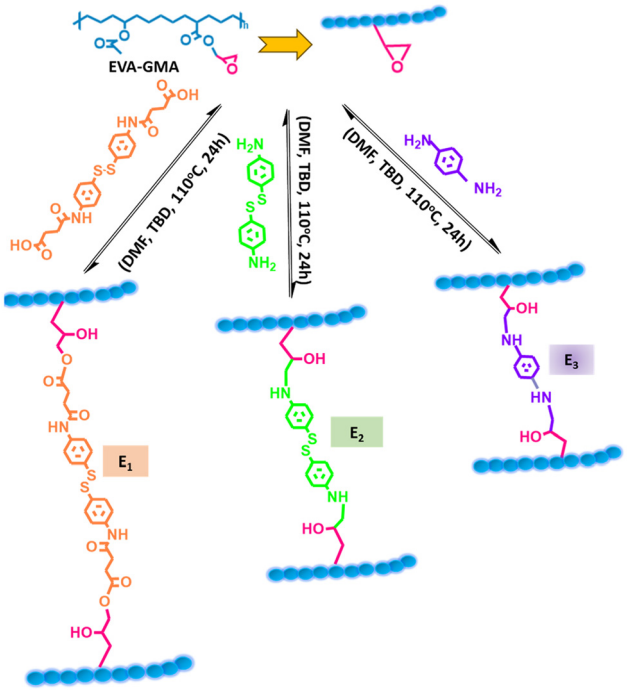

Scheme 2 Schematic representation of various crosslinkers used in this work.

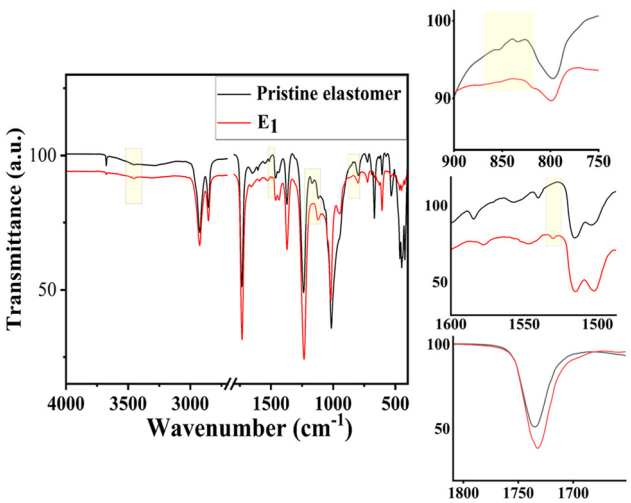

Fig. 1 FTIR spectra of the pristine EVA-GMA elastomer and the same crosslinked with SA-APDS (E_1).

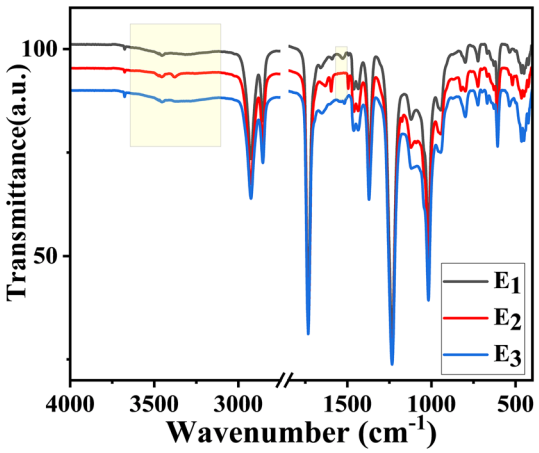

Fig. 2 Comparison of FTIR spectra of E_1 E_2 and E_3.

Study of photoluminescence behaviour

The photoluminescence behaviour of the crosslinked elastomer samples was examined using UV-visible spectroscopy and photoluminescence (PL) spectroscopy. UV-Vis spectra of the crosslinked film samples were recorded, revealing an absorption peak around 390 nm (Fig. S6). This peak is indicative of the presence of specific chromophores within the material. To explore the fluorescence properties, PL spectroscopy was conducted on the crosslinked samples. The emission peak observed at approximately 410 nm confirmed the fluorescence activity of the material under excitation at 390 nm (Fig. 3a).

In particular, sample E_1, where SA-APDS was used as the crosslinker, demonstrated notable fluorescence characteristics. The benzene ring in SA-APDS attached to the amide group on both sides contributed to the extended conjugation in the crosslinker. Fig. 3a illustrates the photoluminescence spectra of the crosslinked samples. In contrast to E_1, samples E_2 and E_3 do not have amide groups, which led to the lack of extended conjugation and hence the absence of fluorescence behaviour. This reduction in extended conjugation resulted in a less stabilised electronic structure, which was less favourable for fluorescence properties. The photographic image of E1 under the irradiation of a UV lamp is shown in Fig. 3b.

Furthermore, time-resolved photoluminescence (TRPL) spectroscopy was employed to investigate the decay profile of the crosslinked elastomeric vitrimer. As shown in Fig. S7a, all samples displayed a sharp rise followed by an exponential decay after pulsed excitation. Notably, sample E_1 exhibited the highest peak intensity and the slowest decay, indicating a longer photoluminescence lifetime. The PL decay profile of the dual dynamic vitrimer was fitted to a double exponential function[43] (eqn (5)).

$$y = A_1 e^{-x/t_1} + A_1 e^{-x/t_1} + y_0 \quad (5)$$

The average lifetime of the elastomeric vitrimer was calculated to be 28.4 ns (Fig. S7b), which indicates that sample E_1 is a suitable candidate for optoelectronic applications.[43,44]

Thermal properties of the crosslinked samples

The thermal properties of the crosslinked vitrimer were studied by DSC and TGA analyses. The pristine elastomers exhibited the lowest glass transition temperature (T_g) at −27 °C, which can be attributed to their unrestricted molecular mobility. As anticipated, the elastomer designated as E_1 displayed the highest T_g, a result of the incorporation of a dual dynamic crosslinker, which significantly restricted the mobility of macromolecular chains. The appearance of the endothermic transition at ~95 °C is attributed to the cleavage of hydrogen bonds (Fig. 4).[45] The presence of two >C═O groups in the crosslinker leads to H-bonding, leading to higher T_g compared to samples E_2 and E_3, as shown in Table S1. The specific design of the dynamic crosslinker, incorporating a longer chain length and flexible methylene segments, enhances the chain flexibility of the compound. As a result, the increase in glass transition temperature (T_g) is not significantly pronounced compared to samples E_2 and E_3.

The decomposition behaviour of the compounds was characterised through TGA and DTG analyses, as shown in Fig. 5a and b, respectively. The EVA-GMA elastomer, which is well known for its excellent resistance to thermal degradation, exhibited a two-

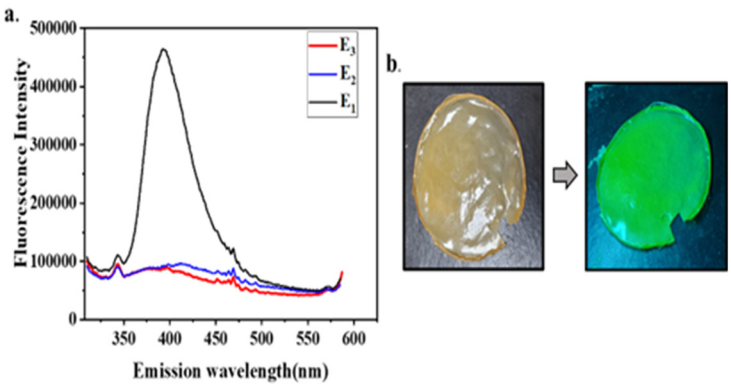

Fig. 3 (a) Photoluminescence spectra of the crosslinked samples; E_1 with SAPDS, E_2 with APDS, and E_3 with AP as the crosslinker (as shown in Scheme 2). (b) The photographic images of E_1 under a UV lamp.

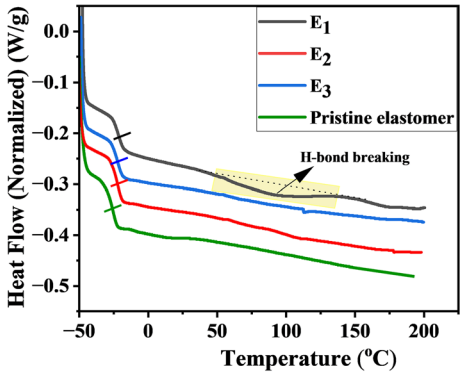

Fig. 4 DSC traces of the pristine and crosslinked samples.

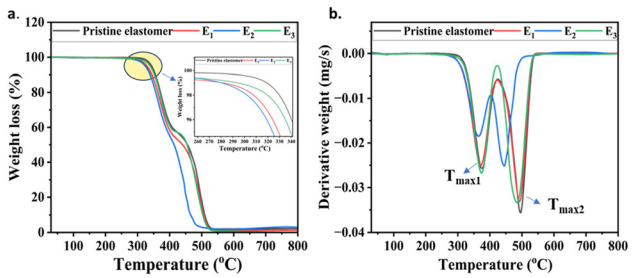

Fig. 5 (a)TGA curves of the pristine elastomer and the crosslinked elastomer; (b) their corresponding DTG plots.

step decomposition process. The first stage of decomposition corresponded to the degradation of the side chains, specifically the vinyl acetate (VA) and glycidyl methacrylate (GMA) groups (T_{max1}, above 360 °C), and the second stage was attributed to the breakdown of the main polymer chain (–CH_2–CH_2–) (T_{max2}, above 440 °C) (Fig. 5b). The pristine elastomer showed the most resistance to thermal degradation. The thermal properties of the crosslinked elastomers were influenced by both the chemical nature of the bonds and the chain length of the crosslinkers. Sample E_3, incorporating a crosslinker with a significantly shorter chain, exhibited the highest thermal stability (Fig. 5a). Although sample E_1 contains a longer crosslinker, the presence of thermally stable amide and ester linkages imparts thermal stability comparable to that of the pristine elastomer and E_3.[46] In contrast, sample E_2, which features a medium chain length crosslinker, undergoes faster thermal degradation due to the presence of thermally labile disulfide and amine linkages.

Mechanical properties of the crosslinked samples

The stress–strain plots of pristine EVA-GMA and the crosslinked samples are shown in Fig. 6a. They indicate that the pristine EVA-GMA has poor tensile strength, although it has excellent weatherability and superior resistance to thermal degradation.[1] The stress–strain analysis revealed that sample E_3 has a tensile strength of less than 0.6 MPa, coupled with minimal elongation at break (EB) of 130%, which was indicative of the sample's inherent stiffness. Similarly, sample E_2 displayed a poor tensile strength of 0.8 MPa and an EB of 850%. Sample E_1 exhibited significantly enhanced tensile properties, with a yield stress of 6.1 MPa and an elongation at break reaching up to 1300%, indicating the super-elastomer-like behaviour with reasonable tensile strength. The enhanced mechanical performance observed in the dual dynamic crosslinked system is attributed to the deliberate integration of complementary dynamic interactions within a well-structured polymer network. There are several reports where researchers have used dual or triple dynamic systems in different polymers to obtain improved properties.[47–49]

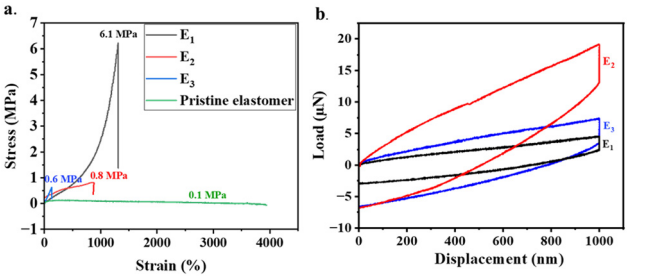

Fig. 6 (a) Tensile properties of the crosslinked elastomer. (b) NINT analysis of the crosslinked samples.

Guo *et al.*[50] demonstrated that a PDMS-based material containing both hydrogen bonds and disulfide bonds showed high stretchability and excellent self-healing performance, attributed to the synergistic effect of covalent and non-covalent interactions. Similarly, Zhang *et al.*[51] reported a supramolecular polymer system containing disulfide bonds, hydrogen bonds, and iron(III)-carboxylate coordination. Their study highlighted that the hierarchical energy dissipation enabled by multiple dynamic linkages, along with high crosslinking density and chain folding, contributed to enhanced mechanical performance. Sarkar *et al.*[48] reported improved mechanical properties in a dual dynamic system of a Diels–Alder reaction and a disulfide metathesis reaction in carboxylated nitrile rubber (XNBR). Herein, the specific structure of the crosslinker enables a synergistic contribution of multiple interactions, including dynamic disulfide exchange, hydrogen bonding through the amide and –COOH groups, and covalent bonding *via* carboxylic acid–epoxy ring-opening reactions. The presence of the methylene spacer enhances the flexibility and chain mobility of the elastomer, contributing to improved extensibility and toughness. Specifically, the incorporation of disulfide bonds, β-hydroxyl ester linkages, and hydrogen bonds enables hierarchical energy dissipation and efficient stress relaxation under deformation.[51] The presence of hydrogen bonding, introduced *via* polar functional groups, contributes significantly to mechanical reinforcement by increasing cohesive energy density, facilitating reversible supramolecular interactions, and promoting improved chain orientation during strain. In contrast, the control sample E_2 incorporates only disulfide and amine functionalities, which limits the extent of hydrogen

bonding and covalent crosslinking, leading to comparatively lower mechanical performance. Sample E_3, crosslinked with a short-chain diamine, forms a rigid and brittle network due to the absence of dynamic bonds and flexible segments, resulting in poor mechanical integrity.

A depth-sensing nanoindentation experiment was conducted to evaluate the surface hardness of the film samples. The hardness values, derived from the force–displacement curves in the nanoindentation study, are summarised in Table S2. Among the samples, E_1 exhibited the highest hardness and modulus values, recorded at 0.9 GPa and 7.3 MPa, respectively. This superior performance is attributed to the dynamic disulfide linkages, hydrogen bonding, covalent interactions (COOH–epoxy), and a flexible methylene spacer in the crosslinker, which contributed to the material's enhanced rigidity and strength. Sample E_3 also demonstrated comparable hardness, although it had lower overall mechanical properties, suggesting that it possessed significant surface hardness due to the tough and brittle nature caused by the short-chain length amine crosslinker. The greater contact depth observed in sample E_2, followed by E_3 and then E_1, further supports the hardness data obtained from the nanoindentation (NINT) analysis. These observations are visually supported by the load–displacement curves presented in Fig. 6b.

The crosslink density in moles per cubic centimetre of the samples was measured using the equilibrium swelling method in toluene and was determined using the Flory–Rehner equation. The details and calculated data are provided in Fig. S6 and Table S3 in the SI. The crosslink density of E_3 (1.45×10^{-3} mol cm^{-3}) is higher than that of E_1, primarily due to the influence of the crosslinker chain length. In this case, the control sample E_3 was crosslinked using AP, which has a significantly shorter chain length compared to the dual dynamic crosslinker (SA-APDS) used in E_1. Generally, crosslink density refers to the number of crosslinks per unit volume, and it influences key material properties such as rigidity, thermal stability, and elongation at break.[46] A shorter crosslinker typically leads to a higher crosslink density. Accordingly, E_3 exhibits a higher crosslink density. However, this increased density results in a more rigid and brittle network, leading to reduced elongation at break and lower tensile strength.

Sol–gel analysis was carried out to obtain the gel fractions of the crosslinked vitrimers (Table S4). The high gel fractions observed for all samples confirm the successful formation of a densely crosslinked network. This also indicates that residual DMF, if any, did not significantly interfere with network integrity or the completeness of the crosslinking reaction.

Stress relaxation experiments

Vitrimers are dynamic materials that exhibit stress relaxation at higher temperatures through reversible covalent bond exchange reactions. These reactions allow the network to flow like a viscoelastic liquid at elevated temperatures while maintaining solid-like properties at lower temperatures.[52,53]

Stress relaxation is a typical feature of vitrimeric materials, as they can easily release deformation at higher temperatures.[54–56] The stress relaxation behaviour of the vitrimers can be explained using the well-known Maxwell model for viscoelastic fluids.[21] The model is expressed in eqn (6).

$$\sigma(t) = \sigma_0 \exp\left(-\frac{E}{\eta}t\right) \quad (6)$$

where σ and σ_0 are the stress at a particular temperature and initial stress, respectively, and E and η are the applied modulus and viscosity of the material, respectively.

To explain this behaviour of the dual dynamic vitrimer (E_1), the stress relaxation experiments were conducted at different temperatures and the decay of stress over time was recorded (Fig. 7a.). At higher temperatures, dynamic covalent bonds in vitrimers undergo rapid exchange reactions, leading to faster stress relaxation over time, and at lower temperatures, the bond exchange reactions slow down, resulting in a reduced rate of stress relaxation. The relaxation time (τ) corresponding to various temperatures is recorded in Table S5.

The dual dynamic vitrimer (E_1) exhibits faster stress relaxation (~38 s) at higher temperatures. It implies an effective rearrangement of the network topology and faster exchange reactions of the dynamic covalent networks. Sample E_2 with a single dynamic crosslink (disulfide bonds) also exhibited a faster stress relaxation time at higher temperatures but showed a longer relaxation time than E_1. The stress relaxation plots of E_2 at various temperatures are provided in Fig. S8. In vitrimers, temperature dependency of the relaxation time is generally expressed in terms of Arrhenius plots (Fig. 7b).[57] The relaxation time follows an Arrhenius-type behaviour given by eqn (7).

$$\tau = \frac{1}{k}\exp\frac{E_a}{RT} \quad (7)$$

The dual dynamic vitrimer showed Arrhenius-like gradual viscosity variations, as observed in vitreous silica.[23] Therefore, stress relaxation was measured at different temperatures to characterize the transesterification reaction. The relaxation time (τ) demonstrated a temperature-dependent behaviour consistent with the Arrhenius law and was accurately described by the Arrhenius equation. The activation energy (E_a) of the dual dynamic vitrimer was calculated to be 46.8 kJ from the Arrhenius plot. Typically, the E_a of epoxy-acid vitrimers ranges

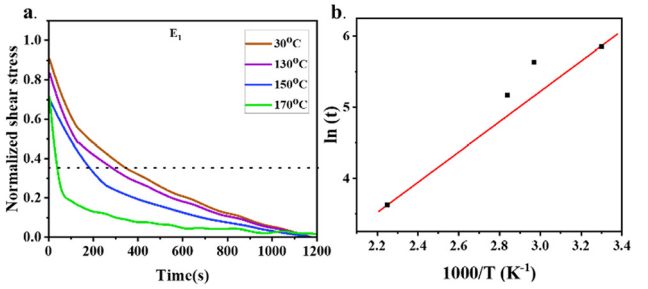

Fig. 7 (a) Normalised stress relaxation plots of the dual dynamic vitrimer. (b) Arrhenius plot of ln(τ) *versus* 1000/T of E_1.

from 30 to 165 kJ; moreover, the presence of the phenyl ring followed by amide linkages in the system enhances the dissociation of disulfide bonds, hence lowering the activation energy.[58–60] Also, the vitrification temperature was estimated to be 83 °C by extrapolating the Arrhenius plot, where the relaxation time reaches 10^6 seconds.[61] The calculations for the estimation of E_a and T_v are provided in the SI.

Study of the dynamic behaviour of the covalent bonds

The stress relaxation experiments were carried out to estimate the rate of dynamic bond recovery. The experiment was initiated by placing the sample in torsion mode at a temperature of 25 °C with no strain and a nominal force of 1 N. Subsequently, a torsional strain of 5% was applied to the sample from 25 °C to 120 °C at a thermal ramp rate of 20 °C min^{-1}, and the sample was held under the same conditions for 20 min. As the next step, the applied 5% strain and the temperature were removed. Throughout the experiment, the shear stress profile was recorded to estimate the rate of dynamic bonds present in the system. The time *versus* shear stress, shear strain and temperature plots are shown in Fig. 8.

In conventional sulphur- or peroxide-cured samples, polymer chains are chemically crosslinked *via* irreversible networks, which restrict their mobility. When subjected to strain, the network deforms, but the crosslinks prevent extensive chain slippage or reorganization. Stress relaxation occurs primarily through mechanisms such as recoiling of chain entanglements and segmental motion. Over time, the stress decreases as these mechanisms allow the polymer chains to rearrange into a more relaxed state. This process is relatively slow and often exhibits a characteristic viscoelastic behaviour, where stress relaxes gradually over time. Unlike traditional crosslinked elastomers, vitrimers possess dynamic networks in which the covalent bonds can break and reform reversibly under appropriate conditions. When subjected to strain in an environment where vitrimer chemistry is activated, the dynamic crosslinks in vitrimers allow for more significant rearrangements of the polymer network compared to conventional elastomers. This dynamic rearrangement enables faster stress relaxation in vitrimers compared to normal elastomers, as the network can adapt and reorganize more readily. The stress relaxation in conventional crosslinked elastomers relies on the mobility of polymer chains within a static network, while vitrimers utilize dynamic covalent bonds to facilitate faster and more extensive rearrangements of their polymer networks, leading to quicker stress relaxation and potentially enhanced mechanical properties. To investigate the dynamic behaviour of vitrimeric crosslinks, a strain-controlled experiment was conducted. In this experiment, strain was initially applied to the sample at room temperature. Subsequently, the temperature of the sample was increased to a range where the dynamic bonds are active. At this elevated temperature, the stress in the dynamic bonds was expected to be alleviated, as the new bonds were formed in the strained position. In the following step, the temperature of the sample was decreased back to room temperature while maintaining the applied strain. At room temperature, the dynamic bonds were no longer dynamic, and they remained oriented according to the strained position. To eliminate the strain at room temperature, a negative stress needed to be applied, which reflects the load supported by the dynamic bonds or the quantity of dynamic bonds present.

In physical terms, at elevated temperatures, dynamic bonds break and reform in the direction of the applied strain, and upon cooling, these newly formed bonds lock into place such that, when the strain is released at room temperature, a restoring shear stress is generated that is proportional to the number of dynamic bonds reformed in the strained configuration.

Herein, the stress measured immediately after the application of strain before the application of temperature can be denoted as $\sigma_{initial}$. And the stress measured after cooling and strain release can be written as $\sigma_{recovered}$. This stress denotes the residual stress that was created at an elevated temperature and locked in after the cooling.

Ideally, in the absence of dynamic bonds in the system,

$$\sigma_{recovered} = 0 \quad (8)$$

And if all the strained bonds had undergone topological network rearrangement,

$$\sigma_{recovered} = \sigma_{initial} \quad (9)$$

Hence,

$$\text{The fraction of dynamic bonds} = \frac{\sigma_{recovered}}{\sigma_{initial}} \quad (10)$$

This relationship can be expressed using eqn (9).

$$\text{Percentage of dynamic bonds} = \frac{\sigma_{recovered}}{\sigma_{initial}} \times 100 \quad (11)$$

The calculation of the percentage of dynamic bonds from the time *versus* shear stress, shear strain and temperature plots is tabulated in Table S6.

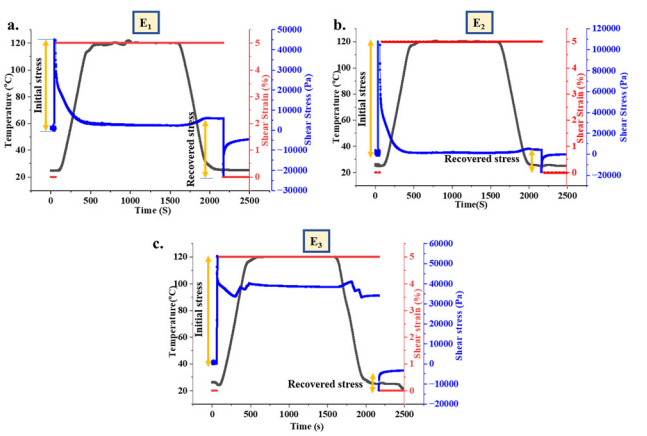

Fig. 8 Dynamic bond recovery test for the crosslinked vitrimers: (a) E_1 with SA-APDS; (b) E_2 with APDS; (c) E_3 with AP as the crosslinker.

Based on eqn (11), the dual dynamic vitrimer E_1 demonstrated the presence of approximately 62% dynamic bonds. In comparison, E_2 exhibited about 20% dynamic bonds, while E_3 showed only 8%. Notably, complete stress relaxation was observed for samples E_1 and E_2, as indicated by the stress falling to zero on the *Y*-axis. This suggests that both E_1 and E_2 experienced full stress relaxation due to their dynamic linkages. On the other hand, sample E_3 did not exhibit complete stress relaxation, which can be attributed to the absence of dynamic linkages in this sample.

Self-healing and reprocessing studies of the dual crosslinked elastomer

Elastomeric vitrimers exhibit good self-healing properties due to their dynamic bonds, which allow the material to autonomically repair minor damage. This capability not only extends the lifespan of elastomeric products but also reduces the need for frequent replacements, making them more sustainable. For conducting the self-healing studies, the crosslinked samples were cut into dumbbell-shaped specimens and their tensile strength was noted. The same samples that were used for evaluating the tensile strength (cut samples) were put together under pressure and were further placed in an oven at 120 °C for 120 min. Subsequently, the temperature of the specimens was brought down to RT, and their tensile strength was noted again.

The healing efficiency was calculated by comparing the tensile strength of the samples before and after the healing process, using the following formula (eqn (12)).

$$\text{Healing efficiency}\,(\%) = \frac{\text{tensile strength of the healed sample}}{\text{tensile strength of the pristine sample}} \times 100 \quad (12)$$

The stress–strain data of the crosslinked and healed samples are presented in Fig. 9a, and the healing efficiency for each sample is summarized in Table S7. The results demonstrated that sample E_1 exhibited good self-healing properties, achieving a healing efficiency of up to 80%. Sample E_2 also showed a commendable self-healing efficiency of approximately 75%. However, sample E_3 did not exhibit any self-healing behaviour, which can be attributed to the absence of any dynamic bonds. The optical microscopy images confirmed significant healing in sample E_1 facilitated by transesterification and disulfide metathesis reactions (Fig. 9c).

Reprocessing studies

Elastomeric vitrimers are characterized by their dynamic covalent bonds, which enable bond exchange reactions under suitable conditions. This unique feature allows the material to be reshaped and reprocessed without degradation, making it suitable for multiple recycling cycles. To assess recyclability, cured samples were cut into small pieces and remoulded at 130 °C for 30 min. The tensile strength of the remoulded samples was then evaluated.

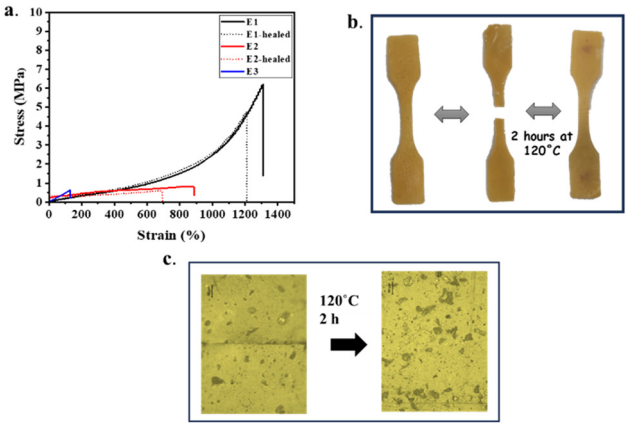

Fig. 9 (a) Stress–strain plots of crosslinked and healed samples. (b) Photographic images of the healing process. (c) Optical microscope image of the dual dynamic vitrimer before healing and after healing.

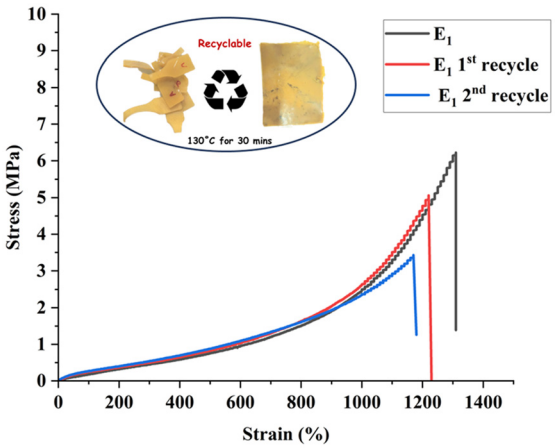

Fig. 10 Stress–strain plot of sample E_1 after the 1st and 2nd recycling.

The dual dynamic vitrimer material, designated as E_1, exhibited impressive recycling efficiency. Remarkably, the material retained up to 84% of its initial tensile strength after the first recycling process and 63% of its original strength after undergoing the second recycling cycle. This retention of mechanical properties underscores the material's durability and resilience, even after multiple recycling processes. The stress–strain plots for the sample following the first and second recycling iterations are presented in Fig. 10, clearly illustrating the material's ability to maintain a significant portion of its mechanical integrity despite repeated processing.

Conclusions

In summary, a dual dynamic crosslinker incorporating disulfide and β-hydroxy ester linkages was synthesized and used to crosslink the commercially available EVA-GMA elastomer. This resulted in a vitrimer-like material based on an epoxy-

functionalized elastomer crosslinked with the dual dynamic crosslinker through transesterification and disulfide bonds. The resultant material demonstrated not only excellent mechanical properties but also significant self-healing and recycling capabilities. The dual dynamic vitrimer achieved a tensile strength of approximately 6.1 MPa and a high elongation at break (EB) of 1300%. The activation energy associated with the dynamic bond exchange was calculated to be 46.8 kJ mol^{-1}, and the vitrification temperature (T_v) was determined to be 83 °C from Arrhenius analysis. It exhibited high dynamic bond content (62%), outstanding self-healing efficiency of ~80%, and retained up to 84% of its tensile strength after the first reprocessing cycle. Interestingly, the crosslinked elastomer also exhibited fluorescence behaviour, attributed to the emission from the fluorogenic conjugated moiety of the synthesized crosslinker. Thus, this new vitrimeric elastomer with fluorescence characteristics can have potential applications in optoelectronic devices such as sensors or flexible display lights, where both mechanical robustness and optical properties are advantageous.

Author contributions

Bhavya Parameswaran: experimental work, methodology, data collection, formal analysis, investigation, interpretation, writing of the original draft, and review & editing. Tuhin Subhra Pal: experimental work and formal analysis. Prof. Nikhil K. Singha: supervision and validation of experimental data and interpretation, overall review, editing, and coordination of the manuscript as the corresponding author.

Conflicts of interest

There are no conflicts to declare.

Data availability

The data that support the findings of this study are available from the authors upon reasonable request.

Supplementary information is available. See DOI: https://doi.org/10.1039/d5lp00127g.

Acknowledgements

BP is grateful to IIT Kharagpur for providing an institute fellowship to carry out the research. We are thankful to Mr Arshad Rahman Parathodika for his assistance while carrying out the DMA analysis. We are thankful to Mr Atif Ansari for his assistance in carrying out the MALDI-TOF analysis. NKS is grateful to Arlanxeo Performance Elastomers, Germany, for providing the EVA-GMA elastomer.

References

1 M. Van Duin, H. Dikland, T. Früh, T. Grob, C. Habmann, N. Sary and R. Schmidit, *Handbook of synthetic rubber*, ARLANXEO, Deutschland, 2020.
2 N. K. Singha and S. C. Jana, *Advances in Thermoplastic Elastomers: Challenges and Opportunities*, Elsevier Science, Netherlands, 2024.
3 U. Kalita, B. Parameswaran and N. K. Singha, *Kirk-Othmer Encycl. Chem. Technol*, 2022, pp. 1–39.
4 A. Y. Coran, *J. Appl. Polym. Sci.*, 2003, **87**, 24–30.
5 B. R. Elling and W. R. Dichtel, *ACS Cent. Sci.*, 2020, **6**, 1488–1496.
6 Y. Liu, Z. Tang, S. Wu and B. Guo, *ACS Macro Lett.*, 2019, **8**, 193–199.
7 W. Alabiso and S. Schlögl, *Polymers*, 2020, **12**(8), 1660.
8 B. Krishnakumar, A. Pucci, P. P. Wadgaonkar, I. Kumar, W. H. Binder and S. Rana, *Chem. Eng. J.*, 2022, **433**, 133261.
9 B. Parameswaran, S. Sarkar, S. Badhra, S. Nair and N. K. Singha, *ACS Appl. Eng. Mater.*, 2024, **2**, 2255–2264.
10 B. Parameswaran and N. K. Singha, in *Toughened Composites*, 2022, vol. 1, pp. 203–216.
11 I. Azcune and I. Odriozola, *Eur. Polym. J.*, 2016, **84**, 147–160.
12 A. V. Tobolsky, W. J. MacKnight and M. Takahashi, *J. Phys. Chem.*, 1964, **68**, 787–790.
13 L. S. Wu, J. Liu, T. T. Wang, Z. H. Luo and Y. N. Zhou, *ACS Appl. Polym. Mater.*, 2024, **6**(20), 12598–12605.
14 H. Wang, Y. Fu, Y. Liu, J. Li, X. Sun and T. Liu, *Eur. Polym. J.*, 2023, **196**, 112309.
15 N. B. Pramanik, P. Mondal, R. Mukherjee and N. K. Singha, *Polymer*, 2017, **119**, 195–205.
16 L. M. Polgar, M. Van Duin, A. A. Broekhuis and F. Picchioni, *Macromolecules*, 2015, **48**, 7096–7105.
17 J. Bai, H. Li, Z. Shi and J. Yin, *Macromolecules*, 2015, **48**, 3539–3546.
18 J. Li, P. Zhang, L. Chen, G. Li, H. Chen, C. Jia, Y. Wu, M. Chen, X. Zhao and P. Song, *Compos. Commun.*, 2020, **22**, 100530.
19 L. Zhu, L. Xu, S. Jie and B. G. Li, *Ind. Eng. Chem. Res.*, 2023, **62**, 2299–2308.
20 M. Das, S. Pal and K. Naskar, *eXPRESS Polym. Lett.*, 2020, **14**, 860–880.
21 S. Sarkar, B. Parameswaran and N. K. Singha, *Eur. Polym. J.*, 2023, **195**, 112194.
22 C. Jin, G. Sinawang, M. Osaki, Y. Zheng, H. Yamaguchi, A. Harada and Y. Takashima, *Polymer*, 2020, **12**, 1393.
23 D. Montarnal, M. Capelot, F. Tournilhac and L. Leibler, *Science*, 2011, **334**, 965–968.
24 T. Liu, B. Zhao and J. Zhang, *Polymer*, 2020, **194**, 122392.
25 J. Luo, Z. Demchuk, X. Zhao, T. Saito, M. Tian, A. P. Sokolov and P. F. Cao, *Matter*, 2022, **5**, 1391–1422.
26 N. J. Van Zee and R. Nicolaÿ, *Prog. Polym. Sci.*, 2020, **104**, 101233.
27 M. Guerre, C. Taplan, J. M. Winne and F. E. Du Prez, *Chem. Sci.*, 2020, **11**, 4855–4870.

28 M. Chen, L. Zhou, Y. Wu, X. Zhao and Y. Zhang, *ACS Macro Lett.*, 2019, **8**, 255–260.
29 A. Vilanova-Pérez, S. Moradi, O. Konuray, X. Ramis, A. Roig and X. Fernández-Francos, *React. Funct. Polym.*, 2024, **195**, 105825.
30 M. Wang, H. Gao, Z. Wang, Y. Mao, J. Yang, B. Wu, L. Jin, C. Zhang, Y. Xia and K. Zhang, *Polymer*, 2022, **248**, 124801.
31 X. Huang, C. Ding, Y. Wang, S. Zhang, X. Duan and H. Ji, *ACS Appl. Mater. Interfaces*, 2024, **16**, 38586–38605.
32 L. Cao, J. Fan, J. Huang and Y. Chen, *J. Mater. Chem. A*, 2019, **7**, 4922–4933.
33 C. Xu, R. Cui, L. Fu and B. Lin, *Compos. Sci. Technol.*, 2018, **167**, 421–430.
34 J. Wang, S. Chen, T. Lin, J. Ke, T. Chen, X. Wu and C. Lin, *RSC Adv.*, 2020, **10**, 39271–39276.
35 Z. Tang, Y. Liu, B. Guo and L. Zhang, *Macromolecules*, 2017, **50**, 7584–7592.
36 L. Cao, J. Fan, J. Huang and Y. Chen, *J. Mater. Chem. A*, 2019, **7**, 4922–4933.
37 J. M. Matxain, J. M. Asua and F. Ruipérez, *Phys. Chem. Chem. Phys.*, 2016, **18**, 1758–1770.
38 H. Y. Tsai, Y. Nakamura, T. Fujita and M. Naito, *Mater. Adv.*, 2020, **1**, 3182–3188.
39 S. K. Raut, P. Mondal, S. Sarkar, B. Parameswaran, S. Bhadra, S. Nair, R. Narain and N. K. Singha, *J. Polym. Sci.*, 2023, 1870–1881.
40 S. Yoon, S. S. Joshi, S. Aracri, Y. Ospina-Yepes, D. Sathe, M. D. Foster, J. Wang and J. M. Eagan, *ACS Appl. Polym. Mater.*, 2025, **7**(7), 4561–4571.
41 N. K. Singha, S. Rimmer and B. Klumperman, *Eur. Polym. J.*, 2004, **40**, 159–163.
42 B. Susrutha, S. Ram and A. K. Tyagi, *J. Mol. Liq.*, 2011, **161**, 132–138.
43 J. Peng, W. Gao, B. K. Gupta, Z. Liu, R. Romero-Aburto, L. Ge, L. Song, L. B. Alemany, X. Zhan, G. Gao, S. A. Vithayathil, B. A. Kaipparettu, A. A. Marti, T. Hayashi, J. J. Zhu and P. M. Ajayan, *Nano Lett.*, 2012, **12**, 844–849.
44 P. Das, M. Bose, S. Ganguly, S. Mondal, A. K. Das, S. Banerjee and N. C. Das, *Nanotechnology*, 2017, **28**(19), 195501.
45 T. S. Pal, B. Parameswaran, S. Koley and N. K. Singha, *ACS Sustain. Chem. Eng.*, 2025, **13**(27), 10339–10353.
46 S. Oprea, V. O. Potolinca and V. Oprea, *Eur. Polym. J.*, 2016, **83**, 161–172.
47 Z. Jiang, A. Bhaskaran, H. M. Aitken, I. C. G. Shackleford and L. A. Connal, *Macromol. Rapid Commun.*, 2019, **40**, 1–10.
48 S. Sarkar, S. L. Banerjee and N. K. Singha, *Macromol. Mater. Eng.*, 2021, **2000626**, 1–13.
49 S. L. Banerjee, S. Samanta, S. Sarkar and N. K. Singha, *J. Mater. Chem. B*, 2020, **8**, 226–243.
50 H. Guo, Y. Han, W. Zhao, J. Yang and L. Zhang, *Nat. Commun.*, 2020, **11**, 1–9.
51 Q. Zhang, C. Y. Shi, D. H. Qu, Y. T. Long, B. L. Feringa and H. Tian, *Sci. Adv.*, 2018, **4**, 1–8.
52 E. Sclarsky, J. Kadlowec and A. J. Vernengo, *Educ. Chem. Eng.*, 2016, **17**, 14–20.
53 L. Imbernon, S. Norvez and L. Leibler, *Macromolecules*, 2016, **49**, 2172–2178.
54 Y. Yang, Y. Xu, Y. Ji and Y. Wei, *Prog. Mater. Sci.*, 2021, **120**, 100710.
55 P. Zhang, P. You, J. Feng, R. Xie, L. Chen, Y. Xiong and P. Song, *Composites, Part A*, 2023, **171**, 107575.
56 A. R. Mahendran, M. Khalifa, G. Wuzella and H. Lammer, *Prog. Polym. Res. Biomed. Energy Spec. Appl.*, 2022, 73–93.
57 S. Tripathi, H. Supriya and S. Bose, *SPE Polym.*, 2024, **5**, 136–150.
58 F. Ruipérez, M. Galdeano, E. Gimenez and J. M. Matxain, *ChemistryOpen*, 2018, **7**, 248–255.
59 F. Cuminet, S. Caillol, É. Dantras, É. Leclerc and V. Ladmiral, *Macromolecules*, 2021, **54**, 3927–3961.
60 B. Aziz, P. Maji, A. R. Parathodika and K. Naskar, *ACS Sustainable Chem. Eng.*, 2024, **12**, 11578–11589.
61 Y. Zhao, T. Qin, C. Jiang, J. Li, Y. Xiong, S. Liu, J. Qin, X. Shi and G. Zhang, *Polymer*, 2023, **265**, 125545.